
Article:
Cole, L.M., Djidja, M.-C., Bluff, J. et al. (5 more authors) (2011) Investigation of protein induction in tumour vascular targeted strategies by MALDI MSI. Methods, 54 (4). pp. 442-453. ISSN 1046-2023

https://doi.org/10.1016/j.ymeth.2011.03.007

Investigation of Protein Induction in Tumour Vascular Targeted Strategies by MALDI-MSI

[1]Cole LM, [1,5]Djidja M-C, [2]Bluff J, [4]Claude E, [1]Carolan VA, [3]Paley M, [2]Tozer GM, [1]Clench MR

[1]Biomedical Research Centre. Sheffield Hallam University, Sheffield, S1 1WB. [2]Tumour Microcirculation Group, Department of Oncology. University of Sheffield, Sheffield S10 2RX. [3]Academic Radiology, Department of Human Metabolism, University of Sheffield, Sheffield, S10 2JF[4]Waters Corporation UK. Atlas Park, Simonsway, Manchester, M22 5PP, [5]The Institute of Cancer Research, London, UK.

Keywords: Matrix Assisted Laser Desorption Ionisation, Mass Spectrometry Imaging, Bottom Up Proteomics, Vascular Disrupting Agent, Combretastatin A-4-3-O-phosphate (CA-4-P/ Zybrestat™) , Haemorrhage, Angiogenesis.

Corresponding author: Professor Malcolm R. Clench, Biomedical Research Centre, Sheffield Hallam University, Howard Street, Sheffield UK. e-mail m.r.clench@shu.ac.uk , FAX +44-1142253066

Abbreviations:

MALDI-MSI	Matrix Assisted Laser Desorption Ionisation- Mass Spectrometry Imaging
MALDI-IMS-MSI	Matrix Assisted Laser Desorption Ionisation- Ion Mobility Separation - Mass Spectrometry Imaging
MALDI-IMS-MS/MS	Matrix Assisted Laser Desorption Ionisation- Ion Mobility Separation – Tandem Mass Spectrometry
CA-4-P	Combretastatin A-4-3-*O*-phosphate (CA-4-P/ Zybrestat™)

1	VEGF	Vascular Endothelial Growth factor
2	PCA-DA	Principle Component Analysis - Discriminant Analysis
3	VDA	Vascular Disrupting Agent
4		
5		
6		
7		
8		
9		
10		
11		
12		
13		
14		
15		
16		
17		
18		
19		
20		

Abstract

Characterising the protein signatures in tumours following vascular-targeted therapy will help determine both treatment response and resistance mechanisms. Here, mass spectrometry imaging and MS/MS with and without ion mobility separation have been used for this purpose in a mouse fibrosarcoma model following treatment with the tubulin-binding tumour vascular disrupting agent, combretastatin A-4-phosphate (CA-4-P). Characterisation of peptides after *in-situ* tissue tryptic digestion was carried out using Matrix Assisted Laser Desorption Ionisation- Mass Spectrometry (MALDI-MS) and Matrix Assisted Laser Desorption Ionisation- Ion Mobility Separation- Mass Spectrometry Imaging (MALDI-IMS-MSI) to observe spatial distribution of peptides. Matrix Assisted Laser Desorption Ionisation-Ion Mobility Separation- Tandem Mass Spectrometry (MALDI-IMS-MS/MS) of peaks was performed to elucidate any pharmacological responses and potential biomarkers. By taking tumour samples at a number of time points after treatment gross changes in the tissue were indicated by the changes in the signal levels of certain peptides. These were identified as arising from haemoglobin and indicated the disruption of the tumour vasculature. It was hoped that the use of PCA-DA would reveal more subtle changes taking place in the tumour samples however these are masked by the dominance of the changes in the haemoglobin signals.

Introduction

The discovery of biomarkers that can be used to determine success of cancer therapy or resistance to it, at an early stage, presents a very complex problem. There are countless biochemical pathways to be considered and the multifaceted characteristics of the cancer cell have also to be taken into account; a cell that can largely evade the host's immune responses and has mastered tissue invasion and anti-cancer drug resistance. Nevertheless good places to start are the 'Hallmarks' of cancer proposed by Hanahan and Weinburg (2000), these include; evasion of apoptosis, self-sufficiency in growth signals, insensitivity to anti-growth signals, tissue invasion and metastasis, limitless replicative potential and sustained angiogenesis. [1]. These capabilities have been used by Lord and Ashworth to classify current anti-cancer drugs [2]. One key point raised in this article is that to decipher the mechanisms of cancer, it should be borne in mind how drugs disturb whole biochemical networks as opposed to solitary pathways. They called this concept, "*drugging the undruggable"*.

One promising class of anti-cancer drug currently under development are vascular disrupting agents (VDAs) [3]. VDAs cause rapid, selective and sustained shutdown of tumour blood flow, which produces drastic effects on the tumour microenvironment. At least part of the blood flow effects are due to direct effects on endothelial cells that line the luminal surface of blood vessels. The article by Kanthou and Tozer [3] describes a proposed mechanism of action for CA-4-P. It is suggested that increased permeability after the administration of CA-4-P is one major factor in the disruption of endothelial organisation. Interference in vascular integrity due to abnormality in the cytoskeleton, subsequently leads to stress fibre formation and endothelial cells become more rounded ('blebbing'). Haemorrhagic necrosis follows, exacerbating the already hypoxic regions within the tumour microenvironment. Remodelling and formation of actin stress fibres is clearly shown in immunofluorescence work by Siemann (2011). The images contained in this article are good examples of the "rounding" of

endothelial cells and “condensation” of the microtubules post CA-4-P treatment. Drug delivery of VDAs is relatively simple due to endothelial positioning near the bloodstream and the diploid target cells are thought not to be directly drug resistant due to low risk of mutations. VDAs have relatively good clinical measurability *i.e.* blood flow and in most cases short-term exposure of a VDA creates sufficient hypoxic conditions to induce necrosis.

However, the use of VDAs to increase hypoxia can also have undesirable consequences [5,6]. Hypoxia-inducible factors (HIF), which are prevalent under hypoxic conditions, cause up-regulation of pro-angiogenic factors such as VEGF. So could VDA amplify the angiogenic process after the creation of an increased hypoxic tumour environment? Hypothetically speaking this could even help the metastatic process ensuring tumour invasion [5]

In addtion to acquired resistance to treatment, the heterogeneous tumour mass could well contain a cell population oblivious to vascular targeted strategies, representing innate resistance [4]. This is supported by the hypothesis that there are four possible micro-vascular phenotypes in existence; normal pre-existing, tumour phenotypic vessels, normal neo-vasculature and abnormal (pathological) neo-vasculature. This could explain why some tumour regions remain unaffected by VDA treatment, including the well-documented viable tumour rim [7]. The viable tumour rim is also thought to achieve evasion through its positioning, adjacent to the non-diseased tissue, which is well supplied with oxygen and essential nutrients [8].

Resistance mechanisms against VDAs are clearly complex and multi-factorial but increased knowledge in this area could provide strategies for future combination therapies. The largest group of VDAs are tubulin binding, microtubule-depolymerising drug such as combretastatin A-4-3-*O*-phosphate (CA-4-P/ Zybrestat^{TM}), which is currently in late stage clinical trials. Combination of CA-4-P or a related compound, Oxi4503 (CA-1-P), with anti-angiogenic therapy such as VEGF receptor tyrosine kinase inhibitors has already shown promise and

novel concepts aimed at targeting circulating angiogenic endothelial progenitor cells have also been proposed. This area has been recently reviewed by Siemann [9]

MALDI-MSI is an advanced analytical tool that allows molecular profiling and imaging of many classes of compounds including; proteins, peptides, lipids, drugs and many other molecules directly from tissue sections. The use of this technique for the study of biological tissue was first described by Caprioli *et al.* in 1997 [10] and it has been improved and adapted for use in many other studies [11-17]. Briefly MALDI-MSI allows the acquisition of multiple single mass spectra across the tissue section at a spatial resolution predefined by the operator (typically 20-200μm). These mass spectra are then combined together in order to generate molecular maps or images which represent the distribution and the relative abundance and/or intensity of a specific ion signal detected within the tissue section. MALDI-MSI has been shown to be a powerful technique for direct protein analysis within tissue sections and in tumour tissue samples, it has been used for discrimination between tumour and non tumour regions with no requirement for predefined targets [18-21]. A recent and exciting development in the technique is the use of "on-tissue" tryptic digestion in order to achieve direct identification of proteins within a tissue section [22-24].

Such molecular profiling and imaging could be described as a bottom-up shotgun approach to protein identification, performed directly on cryo-sectioned tissue samples, rather than through protein extraction methods. The chance to visualise the positioning of peptides within an image generated by MALDI-MSI could indeed advance our knowledge in cancer research studies. Also being able to observe co-localisation of peptides and possibly relate them to disease states can provide complementary information regarding cancerous tissues.

A 2009 article by Djidja *et al* [25] described the profiling and imaging of glucose-regulated protein 78 kDa (Grp78) in pancreatic tumour sections and contains a clear example of peptide identification from the peptide mass fingerprint (PMF) of a tryptic digest. Here *in-situ* tryptic digestion was performed directly onto tissue sections, the resulting PMF allowed

selection of precursor ion for MS/MS. As described within the article, the MALDI images were the first of their kind, with the discussion emphasising the low abundance of this particular heat shock protein. However its importance is not to be underestimated in the aggressiveness, progression and drug resistant nature of tumours. The paper then goes on to describe how the combination of ion mobility and MALDI helped to selectively target specific proteins for imaging. This technique has been called matrix assisted laser desorption ionisation ion mobility separation mass spectrometry imaging (MALDI-IMS-MSI) and its advantages for specific imaging of specific proteins has also been described by others [26].

The experimental work reported here, describes a study, by MALDI-MSI and MALDI-IMS-MSI, of the proteins induced in a mouse transplanted fibrosarcoma model (VEGF120 tumours), at a number of time points, following treatment with CA-4-P. Imaging of peptides signals after *in-situ* tissue tryptic digestion was carried out using MALDI-MS and MALDI-IMS-MSI to observe their spatial distribution. MALDI-IMS-MS/MS of the peptide signals was performed to identify proteins involved in the pharmacodynamic responses to treatment.

Materials and Methods

Materials-

α – Cyano-4-hydroxycinnamic acid CHCA, aniline (ANI), ethanol (EtOH), chloroform ($CHCl_3$), acetonitrile (ACN), Octyl- α / β -glucoside (OcGlc), Tri-fluoroacetic acid (TFA), ammonium calcium carbonate, Haematoxylin, eosin, xylene, DPX mountant were from Sigma-Aldrich (Dorset, UK). Modified sequence-grade trypsin (20µg lyophilised) was obtained from Promega (Southampton, UK).

Tissue samples-

Mice were injected sub-cutaneously in the flank with a 50µl tumour cell suspension containing $1x10^6$ cells in serum-free medium. The cells employed in this study were from the mouse fibrosarcoma cell line, VEGF120. This has been engineered to express only the VEGF120 isoform [27]. Tumours were allowed to grow to approximately 500mm^3, before CA-4-P treatment (a single dose of 100mg/kg i.p). Mice were killed and tumours excised at various time after treatment.

Experimental groups:

Controls (no treatment), n=6 (labelled tumour 1_1 - tumour 1_6), C-A4-P (0 hours after treatment), n=6, (labelled tumour 2_1 - tumour 2_6), , C-A4-P (1/2 hour after treatment), n=6, (labelled tumour 3_1 - tumour 3_6), C-A4-P (6 hours after treatment), n=6, (labelled tumour 4_1 - tumour 4_6), C-A4-P (24 hours after treatment) n=6, (labelled tumour 5_1 - tumour 5_6)

Tissue preparation -

Frozen tissue sections were cut to ~10µm, sections using a Leica CM3050 cryostat (Leica Microsystems). The sections were then freeze thaw mounted on poly-lysine glass slides.

Mounted slides were either used immediately or stored in an airtight tube @ -80℃ for subsequent use.

In situ tissue digestion -

The tissue samples were washed initially with 70% and 90% ethanol respectively for 1 minute then left to dry, after slides were immersed in Chloroform for 10 seconds. Prior to matrix application *In situ* tissue digestion was performed with trypsin solution prepared (from lyophilised trypsin) at 20µg/ml by addition of 50mM ammonium bicarbonate (NH_4HC0_3) pH 8.12, containing 0.5% Octyl-α / β-glucoside (OcGlc). Two automated systems were used for trypsin application. The "Suncollect" (SunChrom, Friedrichsdorf, Germany) automatic pneumatic sprayer was used to spray trypsin in a series of 5 layers employing flow rates of 2µl/min, 3µl/min and 4µl/min. The Portrait™ 630 Multispotter (Labcyte, Sunnyville CA) was used to apply trypsin in a 200 µm - 300 µm array of spots. The sections for MALDI-MS and MALDI-MSI were incubated in a humidity chamber containing H_20 50%: Methanol 50% overnight @ 37℃/ 5% $C0_2$.

Matrix deposition –

The matrix α-cyano-4-hydrocinnamic acid (CHCA) 5mg/ml (Suncollect) or 10mg/ml Portrait™) and aniline in acetonitrile: water: TFA (1:1:0.1) was applied using the Suncollect and Portrait™ 630 Multispotter as above with identical coordinate settings to trypsin deposition to ensure conformity. Aniline was added to the CHCA solution in equimolar amounts to the CHCA added (i.e. 5mg/ml CHCA matrix solution will contain 2.4µl aniline).

Instrumentation -

Peptide mass fingerprints and images were acquired by MALDI-MS/MSI using an Applied Biosystems Q-Star Pulsar *i* hybrid quadrupole time-of-flight mass spectrometer fitted with a variable repetition rate Nd:$YV0_4$ laser set at 5 kHz . Image acquisition was performed using

raster imaging mode at 150µm spatial resolution, Biomap 3.7.5.5 software was used for image generation. To enable simple visual comparison between images all data was normalised to m/z 877 (a peak arising from the αCHCA matrix.) and intensity scales in the BioMap software were all set to the same value.

MALDI-IMS/MS, MALDI-IMS/MSI and MALDI-IMS/MS/MS were performed using a HDMS SYNAPT ™ G2 system (Waters Corporation, Manchester, UK). Drift scope 2.1 software (Waters Corporation, UK. In order to achieve good quality MS/MS spectra, they were acquired manually moving the laser position and adjusting the collision energy to achieve good signal to noise for product ions across the full m/z range of the spectrum. Collision energies were adjusted from 70 – 100 during acquisition and acquisition times were generally of the order of 5-10 seconds per spectrum.

Haematoxylin and eosin staining –

Slides were immersed in Haematoxylin for 1 minute, rinsed in tap water until water runs clear, immerse in 1% Eosin for 30 seconds, rinsed in tap water until water runs clear, dehydration: 50% ethanol for 2min, 70% ethanol for 2 min, 80% ethanol for 2 min, 95% ethanol for 2 min, 4 changes of Xylene applied to each slide for 1 min at a time, mounted with DPX mountant and left to dry in the fumehood overnight.

Data pre-processing

Data lists were exported from Analyst QS software as text files then imported into to SpecAlign to undergo the following data processing; baseline 5, baseline subtraction, smooth, denoise, normalise TIC, remove negative, generate average spectrum, processing spectral alignment, PAFFT correlation method max shift 20. Files were then exported as separate csv. Files and finally exported as text files to import into Marker View software.

Statistical Analysis

PCA-DA was performed using Marker View software, post SpecAlign text files were imported and data was transposed into table format. Minimum intensity 0.1 was selected with maximum number of peaks 20,000. Monoisotopic peaks selected by Marker View were used in the supervised PCA-DA.

Results

A representative peptide mass fingerprint obtained from a tumour from an animal sacrificed immediately after administration of CA-4-P (herafter referred to 0 hours CA-4-P) obtained on the Synapt instrument is shown in Figure 1. These data provide illustration of the vast number of peptides that arise from an *in-situ* tissue tryptic digest, as previously reported by ourselves and others [21-24]. Figure 2 shows IMS/MS/MS data obtained from the peak at m/z 1819.8. This was identified by MASCOT search as arising from Mouse HbAα 42-57 (TYFPHFDVSHGSAQVK) (Table 1). These data (Figure 2 b and 2c) are also a further indication of the advantages of IMS for the identification of "*on-tissue"* generated tryptic peptides. The complexity of the obtained data sets is shown in Figure 2b, where ions arising from doubly charged species and singly charged species are clearly separated by the use of ion mobility and further those singly charged ions arising from peptides and matrix adducts and lipids are also separated. The use of IMS separation prior to MS/MS yielded good quality MS/MS spectra for peptides that produced a high and significant MASCOT score.

Figure 3 (a-e) shows peptide mass fingerprints obtained from the MEF120 tumour tissue sections treated with saline/ CA-4-P in the time course experiments (these data were obtained using the Q-Star instrument). Figure 3a (a) Control/ saline, (b) 0 hours post CA-4-P, (c) 0.5 hours post CA-4-P, (d) 6 hours post CA-4-P, and (e) 24 hours post CA-4-P. The increase in the relative intensity of m/z 1819.3 along with other readily identifiable haemoglobin peptides (e.g. m/z 1529.7 HbAα 18-32 (IGGHGAEYGAEALER), m/z 1274.3

HbAβ 52-41 (LLVVPWTQR) can be clearly seen. This increase in tissue haemoglobin is as would be expected considering the vascular damaging properties of CA-4-P. Due to disruption of the 3D capillary architecture, endothelial cell necrosis, leakage of blood cells into tumour tissues is inevitable. It is clearly illustrated by Figure 4, where MALDI-MS images for the distribution on m/z 1274 (HbAβ 52-41) at each time point are shown along with photographs of the corresponding haematoxylin and eosin stained sections.

The haematoxylin and eosin staining of each VEGF120 serial section was performed after imaging for identification of viable and necrotic tissue and to make observations of the tumour rim. Examples of viable and necrotic tissue are shown in Figure 5. (a) shows a control saline-treated tumour , which is essentially viable, (b) shows a control tumour with a small necrotic region, (c) 0 hours CA-4-P showing viable tissue, (d) 0 hours CA-4-P showing viable and necrotic regions, (e) 0.5 hours after CA-4-P showing viable tissue, (f) 0.5 hours after CA-4-P showing viable and increasing necrotic regions, (g) 6 hours after CA-4-P showing partially viable regions, (h) 6 hours after CA-4-P with haemorrhage and necrosis, (i) 24 hours after CA-4-P treatment showing total necrosis.

Higher magnification images of the H&E staining of tumour rim in the VEGF120 tumour sections are shown in Figure 6 (a) Control/ saline, (b) 0 hours CA-4-P, (c) 0.5 hours CA-4-P, (d) 6 hours CA-4-P, and (e) 24 hours CA-4-P. The H&E tissue sections above reflect the heterogeneous nature of the tumour especially considering the control with no CA-4-P, however the effect of the vascular disrupting agent is still apparent and the 0.5 hour image suggests a good example of the viable tumour resistant rim. In all images viable tumour cells have densely packed nuclei which appear as regions or "organised cells" which stain blue in H&E staining whereas regions of necrosis, due to cell lysis tend to show as a disorganised

region with less blue staining. In these data haemorrhaging also gives a pink colour to the tissue e.g. Fig 5h"

Principle component analysis – discriminant analysis (PCA-DA) was performed to try and correlate peptide induction with dose response and to provide a method of further analysing the PMF data. Figure 7 shows the results of PCA-DA of VEGF120 *In-situ* tryptic digests. 7(a): the scores plot showing groupings and variability between tumour time point spectra, (b): the loadings plot displays the separation and spatial distribution of m/z values in relation to score plot positions, (c): illustrates the variability of two haemoglobin peptides within each tumour section The red arrow on Figure 7(b) indicates m/z 1274 (indicative of haemoglobin β chain) which is associated with the tumour 4 set (6 hours CA-4-P). In Figure 7(b) the green data points are peaks identified as monoisotopic by the MarkerView software and blue data points are peaks which have not been assigned as monoisotopic, these are termed "default" by the software.

The MALDI-MSI images shown in Figure 8 show the distribution of two known peptides in tumour 5_6 i.e. a tumour 24hours after treatment with CA-4-P (a) m/z 1416 from Haemoglobin α chain depicting central necrotic haemorrhage and (b) m/z 1198 corresponding to Actin. The inverse nature of their distribution is striking.

Figure 9 shows examples of overlaid images to show differing spatial distribution and co-registration of peptides using MALDI-MSI. (a) m/z 944 Histone 2A in red (from rainbow) and m/z 1274 Hb in solid green, (b) m/z 1819 Hb in red (from rainbow) and m/z 944 Histone 2A in solid green. The MASCOT scores for the IMS/MS/MS analyses of these peptides are given in Table 1.

Discussion

The potential for investigations into protein induction following drug treatment strategies are phenomenal. Currently one major challenge is the management and analysis of the large amounts of data generated. In each of the peptide mass fingerprints (Figures 1 and 3), on first inspection the spectrum seemed to be very noisy however this could be a signature of a successful tryptic digestion. Therefore the many low abundance peptide signals contained in the apparent noise could house significant proteins such as heat shock proteins and the like, in addition of to the expected and readily visible abundant peptide signals (actin, histones etc). Due to the nature of these results one has to question whether or not each peak is worthy of further scrutiny, or should the vast amount of peaks be simply treated as noise/ interference. The use of ion mobility separation and its associated data extraction software certainly appears to ease this dilemma making many more signals visible for subsequent examination by MS/MS.

In this work the suspected pharmacological response to treatment with CA-4-P of haemorrhaging was investigated (Figure 6). The MALDI-MS images generated from m/z1274 in Figure 4 show a clear increase in Hb with time after treatment with CA-4P. The latter is then confirmed in Figure 5 in the H&E sections. At 6 hours after CA-4-P treatment, the tumour in Figure 5 was partially necrotic and Hb was evident in both necrotic & viable tumour regions. The tumour excised at 24 h was almost completely necrotic. The increase in haemoglobin is also clearly visible in Figure 7(c), the time course plot extracted from the PCA-DA data, where again the increase in m/z 1274 and m/z 1820 can be clearly observed. Many other peptides were observed in this work, including some tentatively identified as arising from VEGF isoforms other than VEGF120. This may be due to infiltration of immune cells [26].This influx and subsequent induction of certain chemokines is a studied response to tumour vascular targeted therapy. In MALDI-MS/MS investigations (results not shown) a

peak at m/z 1334 could indicate Interleukin-6 precursor (IL-6), which has been reported to be induced in tumours after an anti-tumour agent [27], further IMS/MS/MS experiments are required to confirm this.

In PCA-DA analysis of complex data sets, the scores plot (in this case Figure 7a) represents the variance of the original variables, i.e. the obtained sample groups. The loadings plot (in this case Figure 7b) describes the variable behaviour and differences between the observed groups. The PCA-DA analysis of tryptic digest spectra from VEGF120 tumour tissue reported here shows good grouping of the tumour time points (Figure 7a). Confirmation of the increase in haemoglobin due to CA-4-P treatment is given by the association of heamoglobin ions with the 24hr tumour in the loadings plot (Figure 7b) and this is futher shown in Figure 7(c). Further analysis of this large data set is currently underway. The aim of this is to examine whether changes in signals arising from proteins of lower abundance will provide an insight into other pharmacodynamic responses to the treatment.

Conclusions

MALDI-MSI has been used to study the effect of treatment with CA-4-P, a vascular disrupting agent in late stage clinical trials, on mouse VEGF120 tumours. A strategy incorporating "on-tissue" tryptic digestion, MS/MS to identify peptides and ion mobility separation to improve specificity was employed. By taking tumour samples at a number of time points after treatment, gross effects were clearly visible by changes in the expression of certain peptides. These were identified as arising from haemoglobin and indicated the disruption of the tumour vasculature. It was hoped that the use of PCA-DA would reveal more subtle changes taking place in the tumour samples however at present these are masked by the dominance of the changes in the haemoglobin signals. Further statistical analysis of these data is in progress to see if this can be resolved.

Acknowledgements

This work was supported by CR-UK/EPSRC/MRC/NIHR Imaging Programme Grant C1276/A10345

References

1) Hanahan D and Weinberg RA (2000) *The hallmarks of cancer.* Cell. **100.** 57-70
2) Lord CJ and Ashworth A (2010) *Biology-driven cancer drug development: back to the future.* BMC Biology. **8.** (38) 1-12
3) Kanthou and Tozer (2007) *Selective destruction of the tumour vasculature by targeting the endothelial cytoskeleton.* Drug discovery today: Therapeutic strategies. **4.** (4) 237-243
4) Thorpe PE, Chaplin DJ, Blakey DC (2003) *The first international conference on vascular targeting: Meeting overview.* Cancer Research. **63.** 1144-1147
5) Zhi-chao SI, Jie L (2008) *What 'helps' tumours evade vascular targeting treatment?* Chinese Medical Journal. **121.** (9) 844-849
6) Tozer GM, Kanthou C, Lewis G, Prise VE, Vojnovic B, Hill A (2008) *Tumour vascular disrupting agents: combating treatment resistance.* The British Journal of Radiology. **81.** S12-S20
7) Abdollahi A, Folkman J (2010) *Evading tumour evasion: Current concepts and perspectives of anti-angiogenic cancer therapy.* Drug Resistance Updates. **13.** 16-28
8) Kanthou C and Tozer GM (2009) Microtubule depolymerizing vascular disrupting agents: novel therapeutic agents for oncology and other pathologies International Journal of Experimental Pathology 80. 284-294.

9) Siemann W. (2009) *"Vascular targeted therapies in oncology"* Cell and Tissue Research 335. 241-248.

10) Caprioli, R. M., Farmer T.B. and Gile J. (1997) Molecular Imaging of Biological Samples: Localization of Peptides and Proteins Using MALDI-TOF MS *Anal. Chem*. 69, 4751-4760.

11) Chaurand, P.; Cornett, D. S.; Caprioli, R. M. (2006) Molecular imaging of thin mammalian tissue sections by mass spectrometry *Curr. Opin. Biotechnol. 17,* 431-436.

12) Chaurand, P.; Fouchécourt, S.; DaGue, B. B.; Xu, B. J.; Reyzer, M. L.; Orgebin-Crist, M.; Caprioli, R. M. (2003) Profiling and imaging proteins in the mouse epididymis by imaging mass spectrometry *Proteomics*, *3,* 2221-2239.

13) Stoeckli, M.; Staab, D.; Schweitzer, A.; Gardiner, J.; Seebach, D. (2007) Imaging of a beta-peptide distribution in whole-body mice sections by MALDI mass spectrometry *J. Am. Soc. Mass Spectrom. 18,* 1921-1924.

14) Burrell, M.; Earnshaw, C.; Clench, M. (2007) Imaging Matrix Assisted Laser Desorption Ionization Mass Spectrometry: a technique to map plant metabolites within tissues at high spatial resolution *J. Exp. Bot. 58,* 757-763.

15) Djidja, M.; Carolan, V.; Loadman, P. M.; Clench, M. R. (2008) Method development for protein profiling in biological tissues by matrix-assisted laser desorption/ionisation mass spectrometry imaging *Rapid Commun. Mass Spectrom. 22,* 1615-1618.

16) Trim, P. J.; Atkinson, S. J.; Princivalle, A. P.; Marshall, P. S.; West, A.; Clench, M. R. (2008) Matrix-assisted laser desorption/ionisation mass spectrometry imaging of lipids in rat brain tissue with integrated unsupervised and supervised multivariant statistical analysis *Rapid Commun. Mass. Spectrom. 22,* 1503-1509.

17) Fournier, I.; Wisztorski, M.; Salzet, M. (2008) Tissue imaging using MALDI-MS: a new frontier of histopathology proteomics *Expert Rev Proteomics 5,* 413-424.

18) Schwartz, S. A.; Weil, R. J.; Johnson, M. D.; Toms, S. A.; Caprioli, R. M. Protein profiling in brain tumors using mass spectrometry: feasibility of a new technique for the analysis of protein expression *Clin. Cancer Res.* **2004**, *10,* 981-987.

19) Chaurand, P.; DaGue, B. B.; Pearsall, R. S.; Threadgill, D. W.; Caprioli, R. M. Profiling proteins from azoxymethane-induced colon tumors at the molecular level by matrix-assisted laser desorption/ionization mass spectrometry *Proteomics* **2001**, *1,* 1320-1326.

20) Lemaire, R.; Menguellet, S. A.; Stauber, J.; Marchaudon, V.; Lucot, J.; Collinet, P.; Farine, M.; Vinatier, D.; Day, R.; Ducoroy, P.; Salzet, M.; Fournier, I. Specific MALDI imaging and profiling for biomarker hunting and validation: fragment of the 11S proteasome activator complex, Reg alpha fragment, is a new potential ovary cancer biomarker J. Proteome. Res. 2007, 6, 4127-4134.

21) Schwamborn, K.; Krieg, R. C.; Reska, M.; Jakse, G.; Knuechel, R.; Wellmann, A. Identifying prostate carcinoma by MALDI-Imaging Int. J. Mol. Med. 2007, 20, 155-159.

22) Lemaire, R.; Desmons, A.; Tabet, J. C.; Day, R.; Salzet, M.; Fournier, I. Direct analysis and MALDI imaging of formalin-fixed, paraffin-embedded tissue sections J. Proteome Res. 2007, 6, 1295-1305.

23) Shimma, S.; Furuta, M.; Ichimura, K.; Yoshida, Y.; Setou, M. A Novel Approach to in situ Proteome Analysis Using Chemical Inkjet Printing Technology and MALDI-QIT-TOF Tandem Mass Spectrometer J. Mass Spectrom. Soc. Jpn. 2006, 54, 133-140.

24) Groseclose, M. R.; Andersson, M.; Hardesty, W. M.; Caprioli, R. M. Identification of proteins directly from tissue: in situ tryptic digestions coupled with imaging mass spectrometry J. Mass Spectrom. 2007, 42, 254-262.

25) Djidja M-C, Claude E, Snel MF, Scriven P, Francese S, Carolan V, Clench MR (2009) *Maldi-ion mobility separation-mass spectrometry imaging of glucose-regulated protein 78 kDa (Grp78) in human formalin fixed paraffin-embedded pancreatic adenocarcinoma tissue sections.* Journal of Proteome Research. **8.** (10) 4876-4884

26) McDonnell LA, Corthals GL, Willems SM, Remoortere van A, Zeijl van RJM, Deelder AM (2010) *Peptide and protein imaging mass spectrometry in cancer research.* Journal of Proteomics. **73.** 1921-1944

27) Wang L-CS, Thomsen L, Sutherland R, Reddy CB, Tijono SM, Chen C-JJ, Angel CE, Dunbar PR and Ching LM (2009) Neutrophil Influx and Chemokine Production during the early phases of the anti-tumour response to the vasculature disrupting agent DMXAA (ASA404). Neoplasia 11. 793-803.

28) Tozer GM, Akerman S, Cross N.A. *et al* (2008) *"Blood Vessel Maturation and Response to Vascular-Disrupting Therapy in Single Vascular Endothelial Growth Factor-A Isoform–Producing Tumors"* Cancer Research 68, 2301-2311.

Table 1: Identities and MASCOT scores from the IMS/MS/MS analyses of the peptide signals imaged.

Protein	Accession number	Observed m/z with MALDI-MSI	Sequence	Score	MASCOT threshold score at 95% significance
Haemoglobin subunit alpha	P01942	2836.4	VADALASAAGHLDDLPGALSALSDLHAHK	87	>40
Haemoglobin alpha chain	P01942	1819.8	TYFPHFDVSHGSAQVK	106	>36
Haemoglobin alpha chain	P01942?	1416.7	GGHGAEYGAEALER	87	>43
Haemoglobin beta chain	P02088	1302.6	VNSDEVGGEALGR	79	>38
Histone H3	P68433	1032.6	YRPGTVALR	11	>10
Histone 2A	Q8CGP5	944.5	AGLQFPVGR	24	>19

Legends to Figures

Figure 1: Representative Peptide Mass Fingerprint (PMF) arising from an on-tissue digest of a VEGF120 tumour 0 hours after dosing with 100mg/kg i.p, CA-4-P. Prior to matrix application *In situ* tissue digestion was performed with trypsin solution prepared (from lyophilised trypsin) at 20µg/ml by addition of 50mM ammonium calcium carbonate (NH_4CaC0_3) pH 8.12, containing 0.5% Octyl- α / β -glucoside (OcGlc). The matrix employed was α -cyano-4-hydroxycinnamic acid (CHCA) 5mg/ml and aniline in acetonitrile: water: TFA (1:1:0.1).

Figure 2a: IMS/MS/MS data obtained from the peak observed in Figure 1 at m/z 1819.3. This was identified by MASCOT search as arising from Mouse HbAα 42-57 (TYFPHFDVSHGSAQVK).

Figure 2b: A Driftscope plot of a tumour section 24 hrs post CA-4-P showing the ion mobility separation as a function of driftime. Possible trend lines of doubly charged singly charged and suspected matrix adduct ions/ lipids are indicated.

Figure 2c: Zoomed in Driftscope plot shows ion mobility separation of ion of interest Haemoglobin subunit alpha m/z 1819.8 and C13 as shown on chromatogram directly below.

Figure3: Peptide mass fingerprints obtained from the VEGF120 tumour tissue sections treated with saline/ 100mg/kg i.p, CA-4-P time course experiments. Figure 3a (a) Control/

saline, (b) 0 hours post CA-4-P,(c) 0.5 hours post CA-4-P, (d) 6 hours post CA-4-P, (e) 24 hours post CA-4-P.

Figure 4: MALDI-MS images for the distribution of m/z 1274 (HbAβ 52-41) at (a)Control/ saline, (b) 0 hours post CA-4-P (c) 0.5 hours post CA-4-P, (d) 6 hours post CA-4-P, (e) 24 hours post CA-4-P along with photographs of the corresponding haematoxylin and eosin stained sections.

Figure 5: Haematoxylin and eosin stained sections (a) Control/ saline showing viable tissue, (b) Control showing, a small necrotic region, (c) 0 hours CA-4-P showing viable tissue, (d) 0 hours CA-4-P showing viable and necrotic regions, (e) 0.5 hours CA-4-P showing viable tissue, (f) 0.5 hours showing viable and increasing necrotic regions, (g) 6 hours CA-4-P showing partially viable regions, (h) 6 hours CA-4-P with haemorrhaging and necrosis, (i) 24 hours after CA-4-P treatment showing total necrosis.

Figure 6: Higher magnification images of the H&E staining of tumour rim in the VEGF120 tumour sections are shown in Figure 6 (a) Control/ saline, (b) 0 hours CA-4-P, (c) 0.5 hours CA-4-P, (d) 6 hours CA-4-P, (e) 24 hours CA-4-P. The 0.5 hour image displays a good example of the viable tumour resistant rim.

Figure 7: PCA-DA of VEGF120 tumour *In-situ* tryptic digests. (a): the scores plot showing groupings and variability between tumour time point spectra, (b): the loadings plot displaying the separation and spatial distribution of m/z values in relation to score plot positions, (c): illustrates the variability of two haemoglobin peptides within each tumour section The red arrow on Figure 7(b) indicates m/z 1274 (indicative of haemoglobin β chain) which is associated with the tumour 4 set (6 hours CA-4-P).

Figure 8: The distribution of two known peptides in tumour 5_6 i.e. a tumour 24hours after treatment with CA-4-P (a) m/z 1416 from Haemoglobin α chain depicting central necrotic haemorrhage and (b) m/z 1198 corresponding to Actin. The inverse nature of their distribution is striking.

Figure 9: Overlaid MALDI-MSI images showing differing spatial distribution and co-registration of peptides. (a) m/z 944 Histone 2A in red and m/z 1274 Hb in solid green, (b) m/z 1819 Hb in red and m/z 944 Histone 2A in solid green.

Figure 1

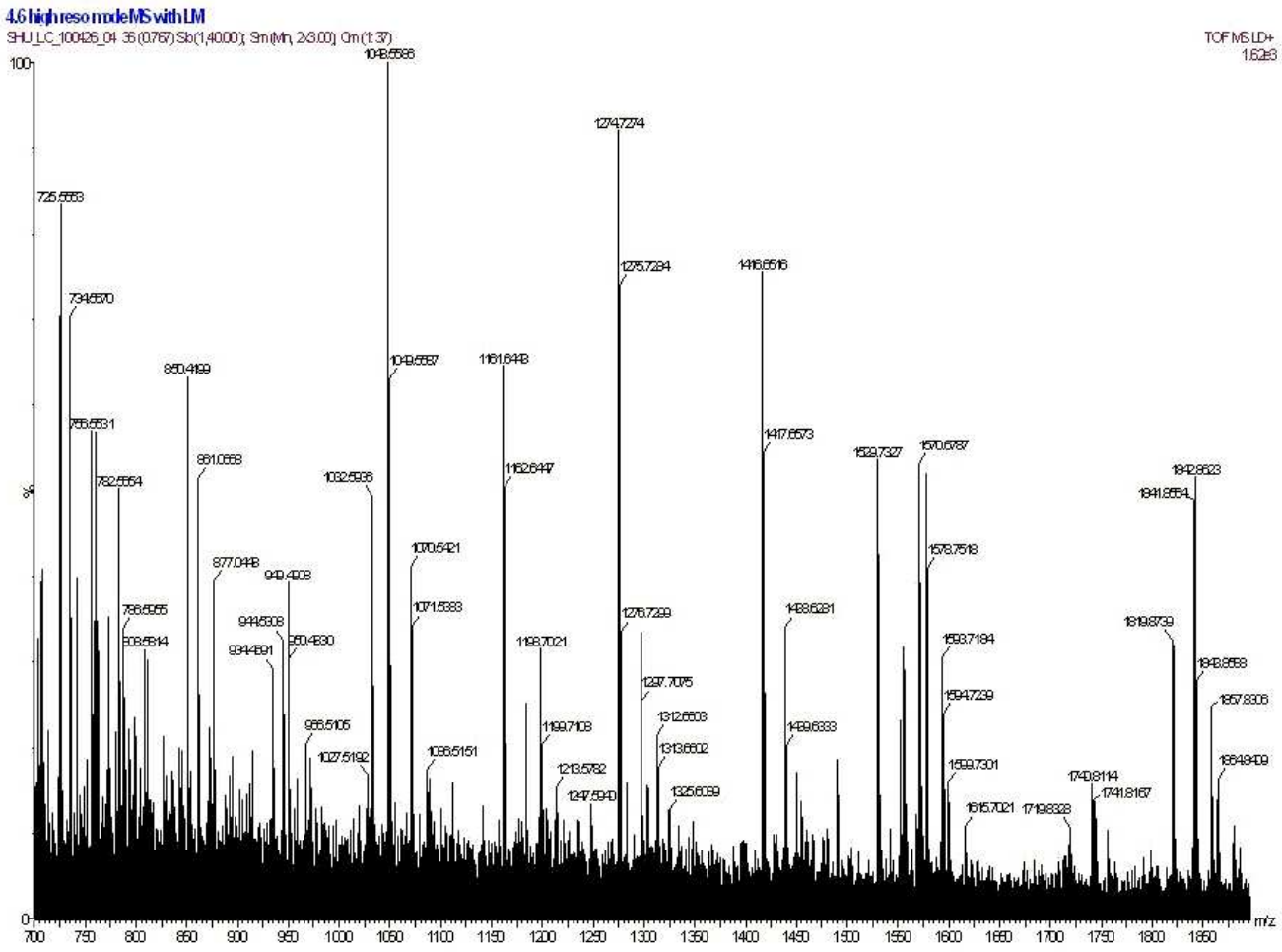
4.6 high resolution MS with LM
SHU_LC_100426_04 36 (0.767) Sb (1,40.000); Sm (Mn, 2x3.00); Cm (1:37)
TOF MS LD+
1.62e3
100
%
0
1048.5586
1274.7274
725.5553
1275.7284
1416.6516
794.5570
1049.5587
1161.6448
850.4199
1417.6573
766.5531
1529.7327
1570.6787
851.0668
1162.6447
782.5564
1942.8523
1941.8554
1032.5536
1578.7518
1070.5421
877.0448
949.4208
1071.5583
1488.6281
766.5555
1276.7299
944.5608
808.5514
1819.8739
1199.7021
1593.7184
984.4691
950.4830
1237.7075
1848.8568
1312.6603
1594.7239
1199.7103
1857.8305
955.5105
1313.6602
1489.6333
1027.5192
1086.5151
1213.5782
1599.7301
1864.8409
1247.5940
1325.6039
1740.8114
1741.8167
1615.7021
1719.8328
m/z
700
750
800
850
900
950
1000
1050
1100
1150
1200
1250
1300
1350
1400
1450
1500
1550
1600
1650
1700
1750
1800
1850

Figure 2a

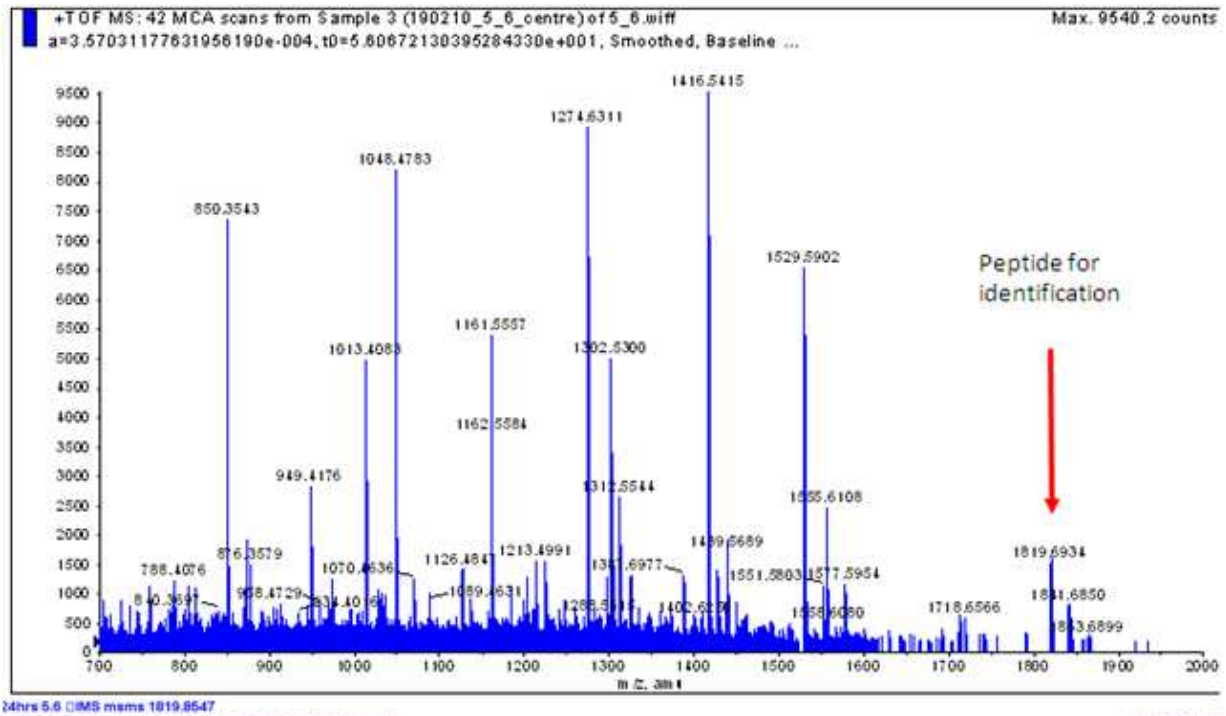
+TOF MS: 42 MCA scans from Sample 3 (190210_5_6_centre) of 5_6.wiff
Max. 9540.2 counts
Peptide for identification
1819.6934
1416.5415
1274.6311
1048.4783
850.3543
1529.5902
1161.5557
1013.4083
1302.5300
1162.5584
949.4176
1312.5544
1555.6108
1213.4991
1126.484
1070.4536
876.3579
788.4076
1718.6566
1841.6850
1883.6899

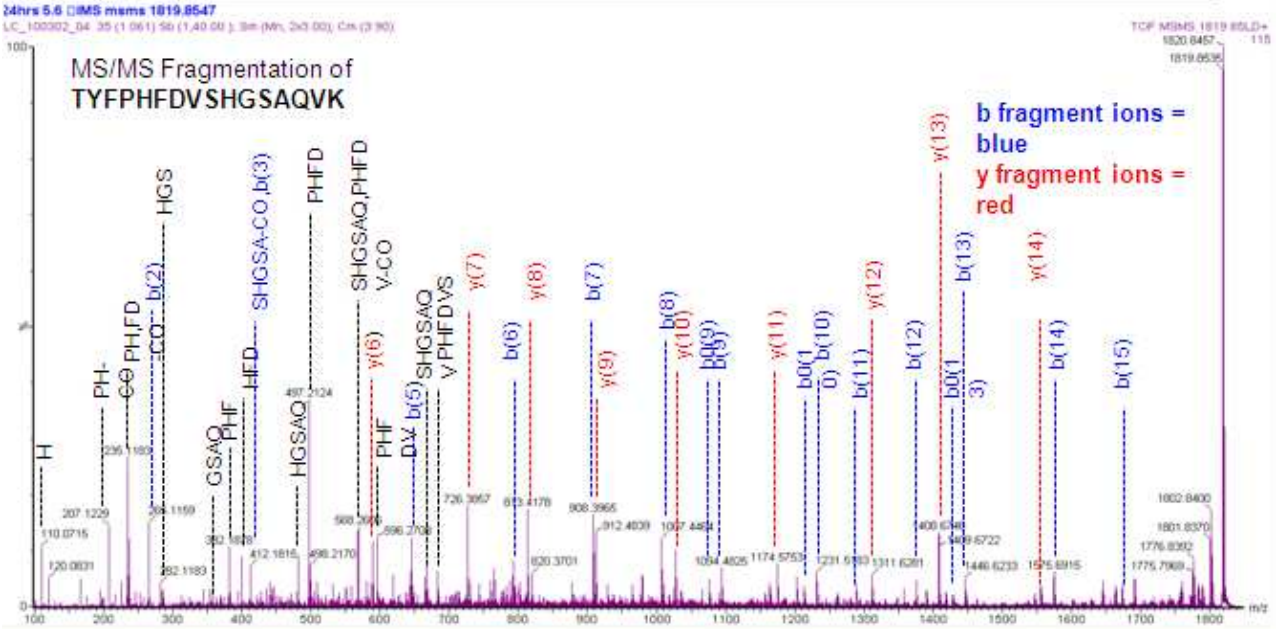
MS/MS Fragmentation of
TYFPHFDVSHGSAQVK
b fragment ions = blue
y fragment ions = red

Figure 2b

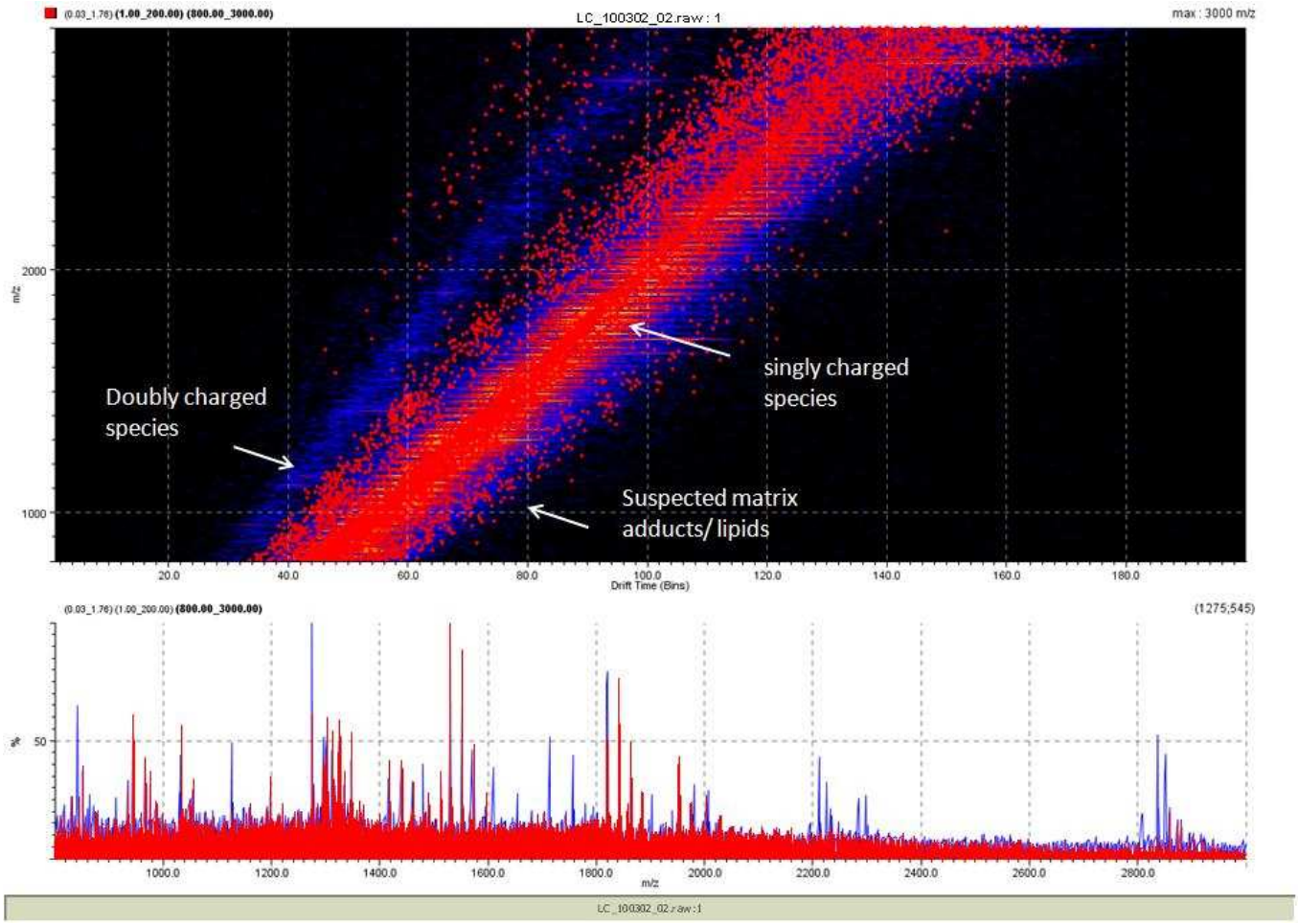
LC_100302_02.raw : 1
max : 3000 m/z
Doubly charged species
singly charged species
Suspected matrix adducts/ lipids
Drift Time (Bins)
m/z
(1275;545)

Figure 2c

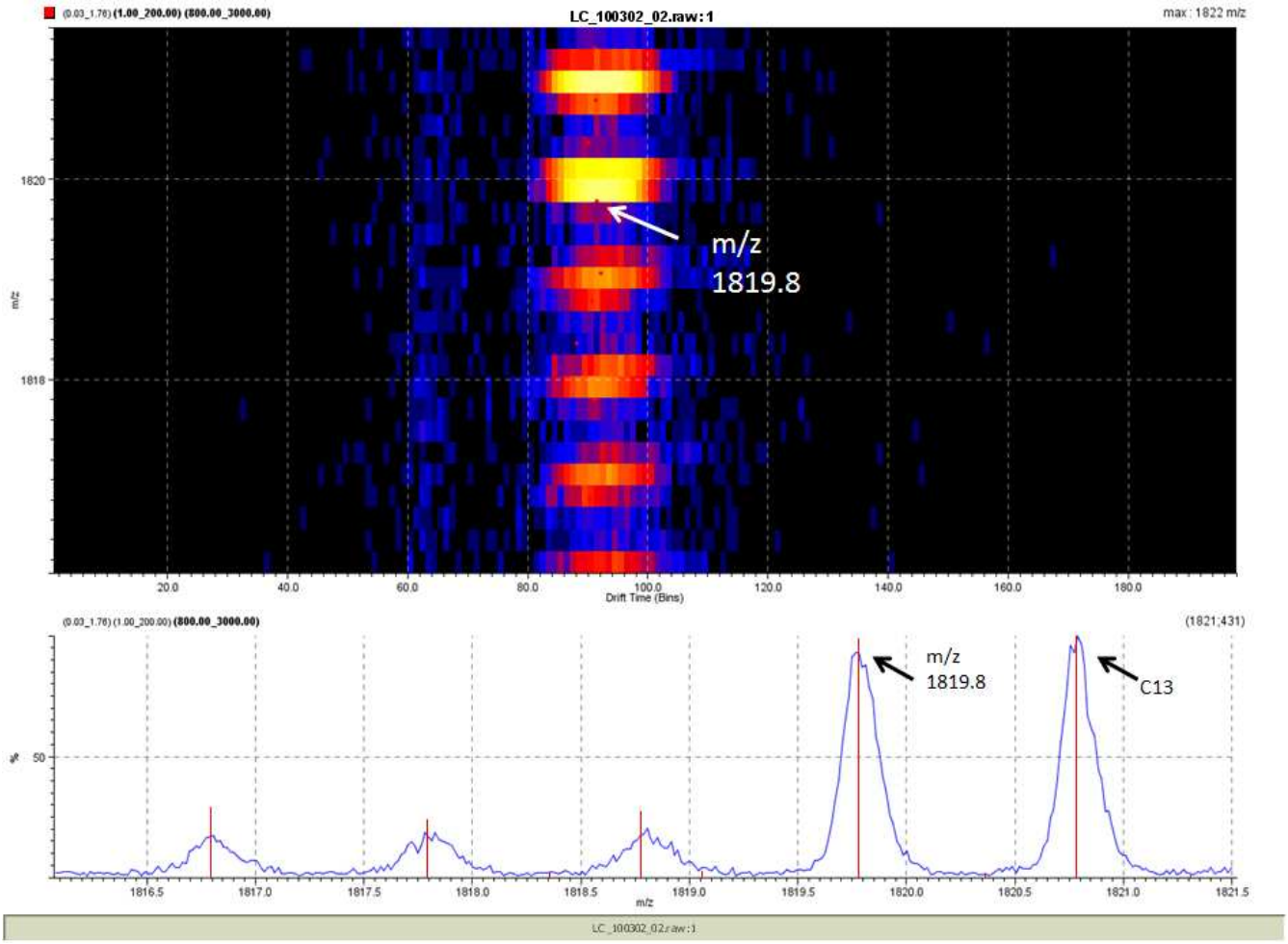
LC_100302_02.raw:1
max : 1822 m/z
m/z
1819.8
Drift Time (Bins)
(1821;431)
m/z
1819.8
C13
m/z

Figure 3a

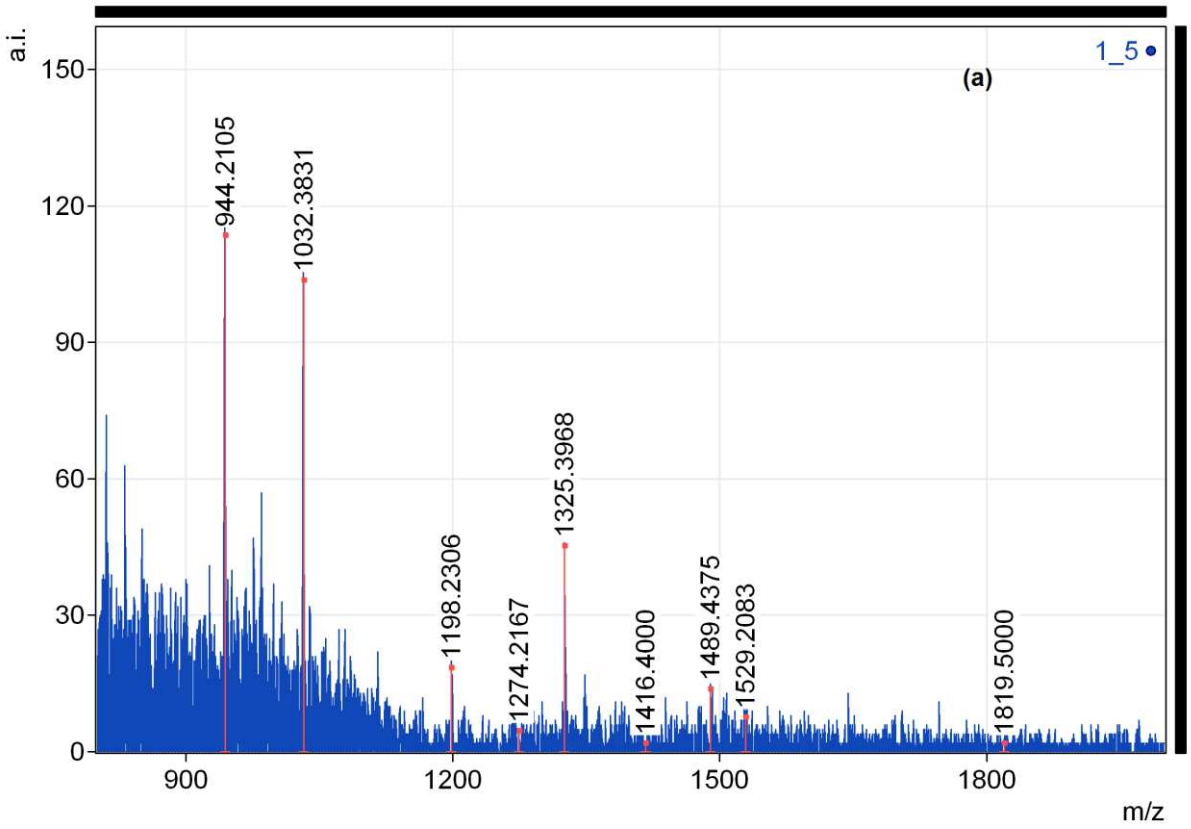
a.i.
150
120
90
60
30
0
900
1200
1500
1800
m/z
1_5
(a)
944.2105
1032.3831
1198.2306
1274.2167
1325.3968
1416.4000
1489.4375
1529.2083
1819.5000

Figure 3b

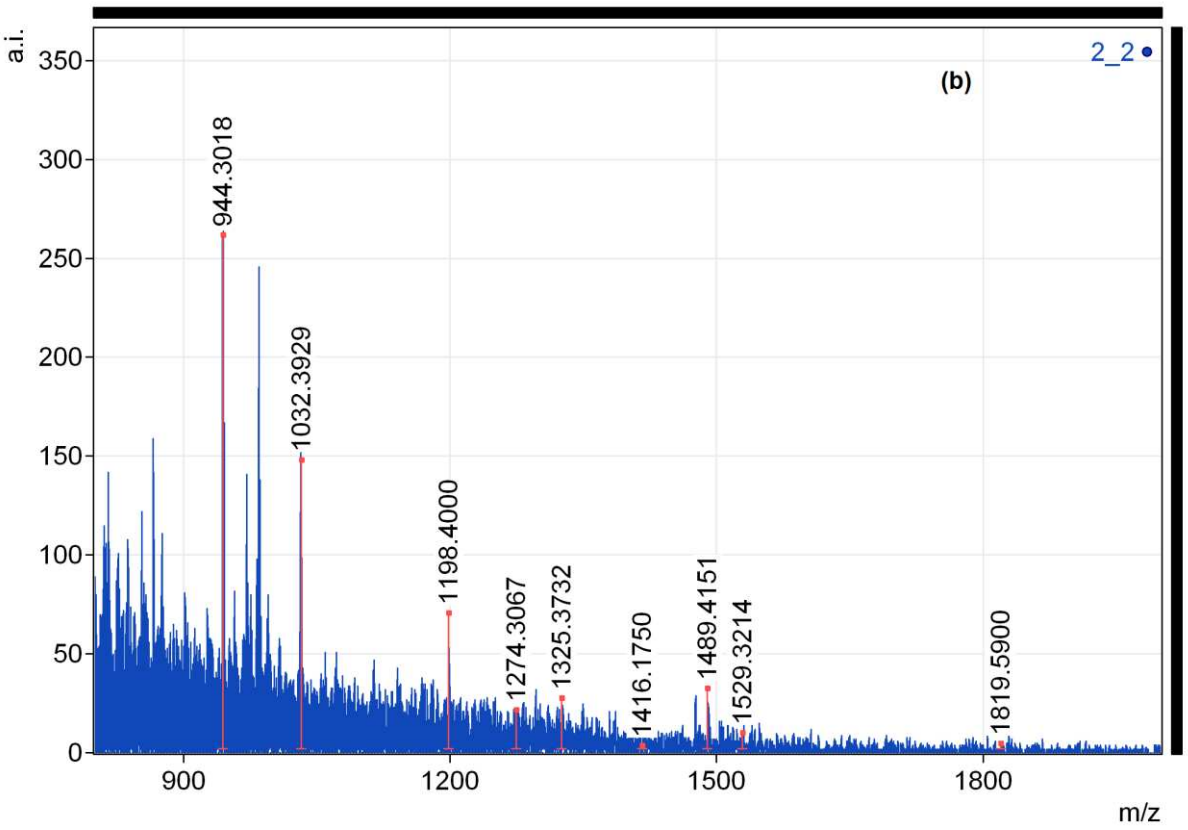
a.i.
350
300
250
200
150
100
50
0
2_2
(b)
944.3018
1032.3929
1198.4000
1274.3067
1325.3732
1416.1750
1489.4151
1529.3214
1819.5900
900
1200
1500
1800
m/z

Figure 3c

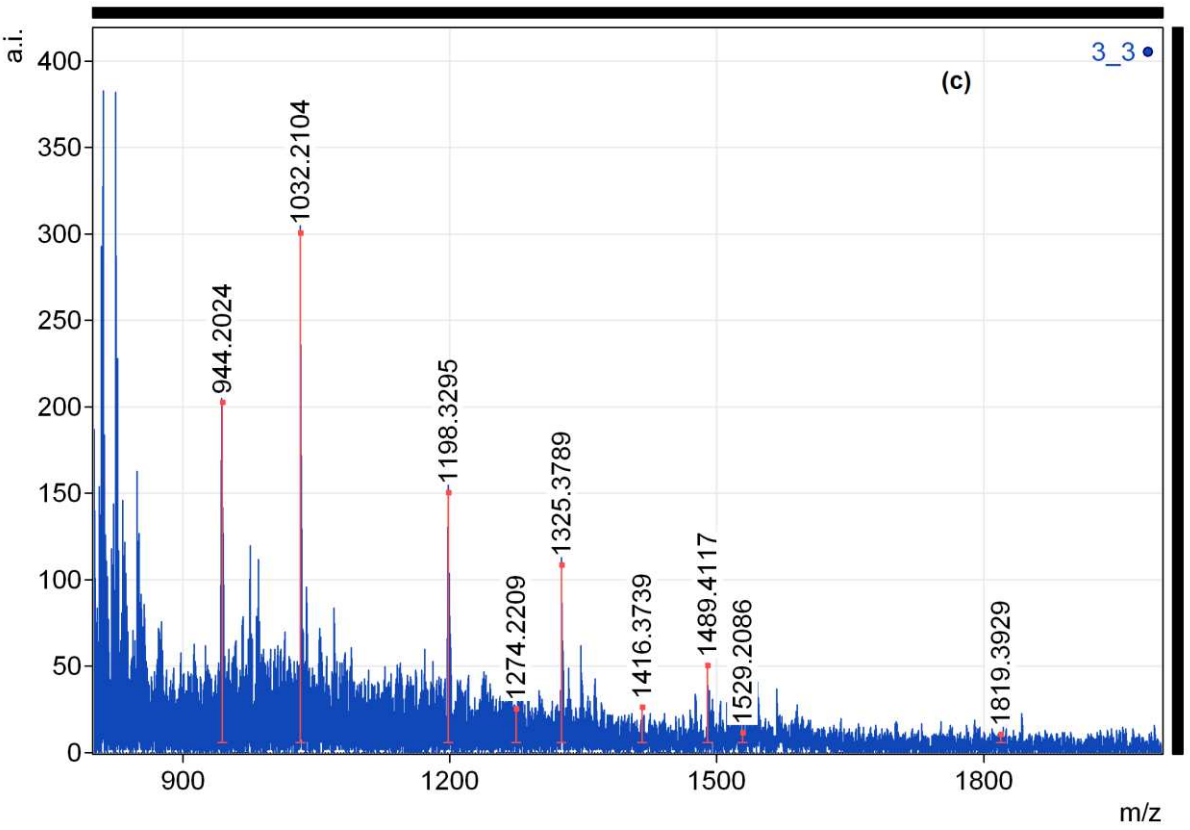
a.i.
400
350
300
250
200
150
100
50
0
3_3
(c)
1032.2104
944.2024
1198.3295
1325.3789
1274.2209
1416.3739
1489.4117
1529.2086
1819.3929
900
1200
1500
1800
m/z

Figure 3d

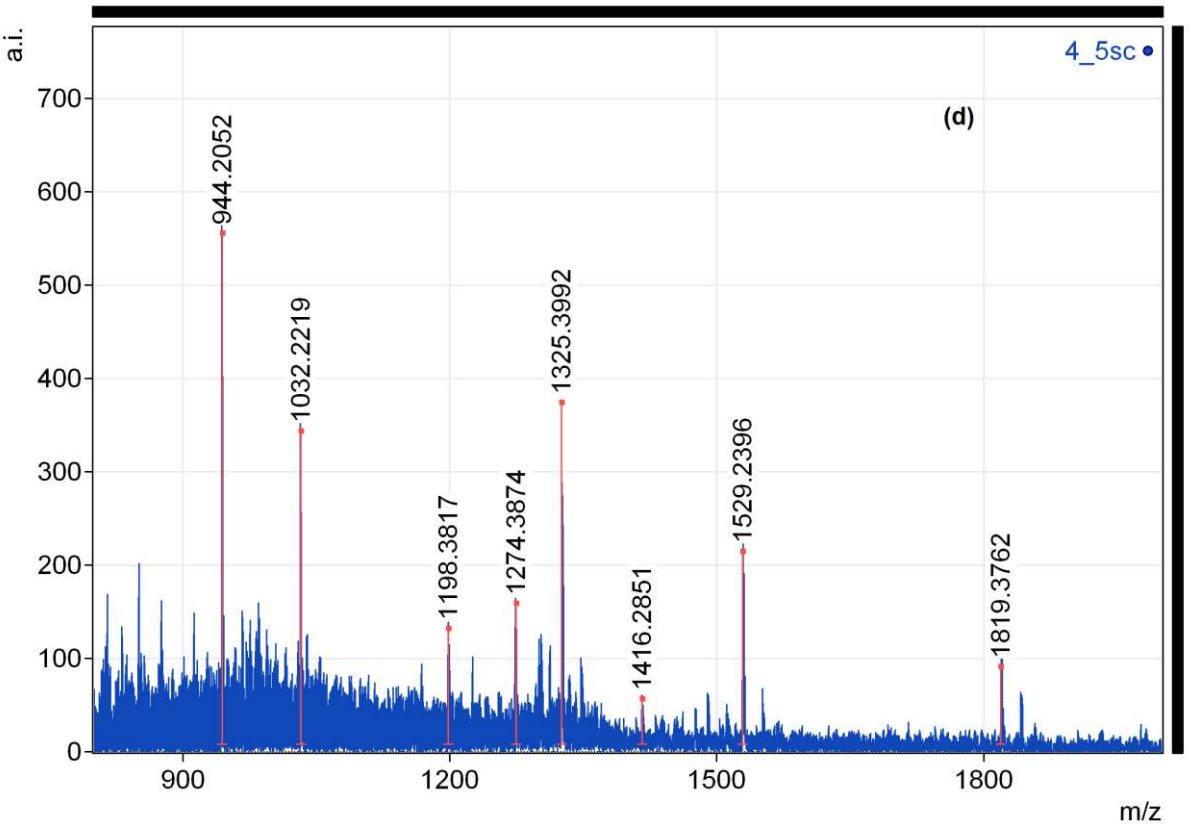
a.i.
4_5sc
(d)
944.2052
1032.2219
1198.3817
1274.3874
1325.3992
1416.2851
1529.2396
1819.3762
700
600
500
400
300
200
100
0
900
1200
1500
1800
m/z

Figure 3e

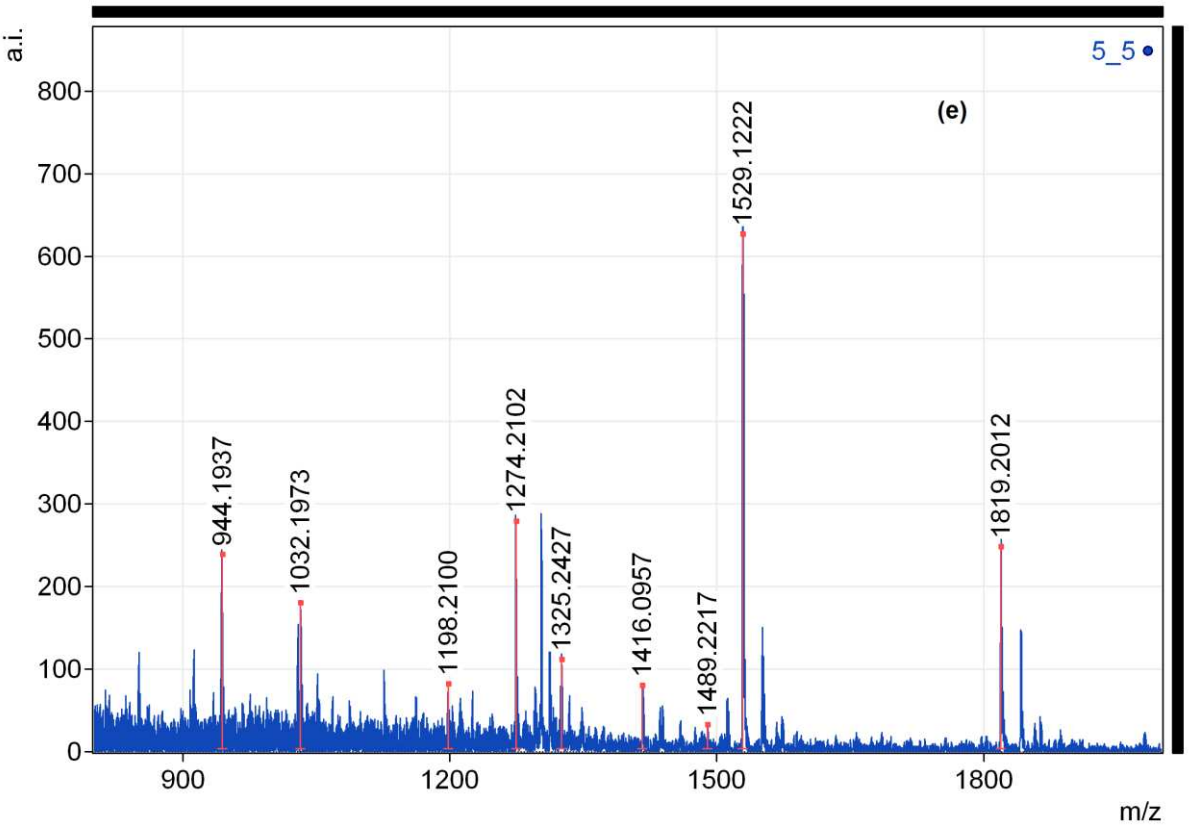
a.i.
5_5
(e)
800
700
600
500
400
300
200
100
0
944.1937
1032.1973
1198.2100
1274.2102
1325.2427
1416.0957
1489.2217
1529.1222
1819.2012
900
1200
1500
1800
m/z

1 Figure 4

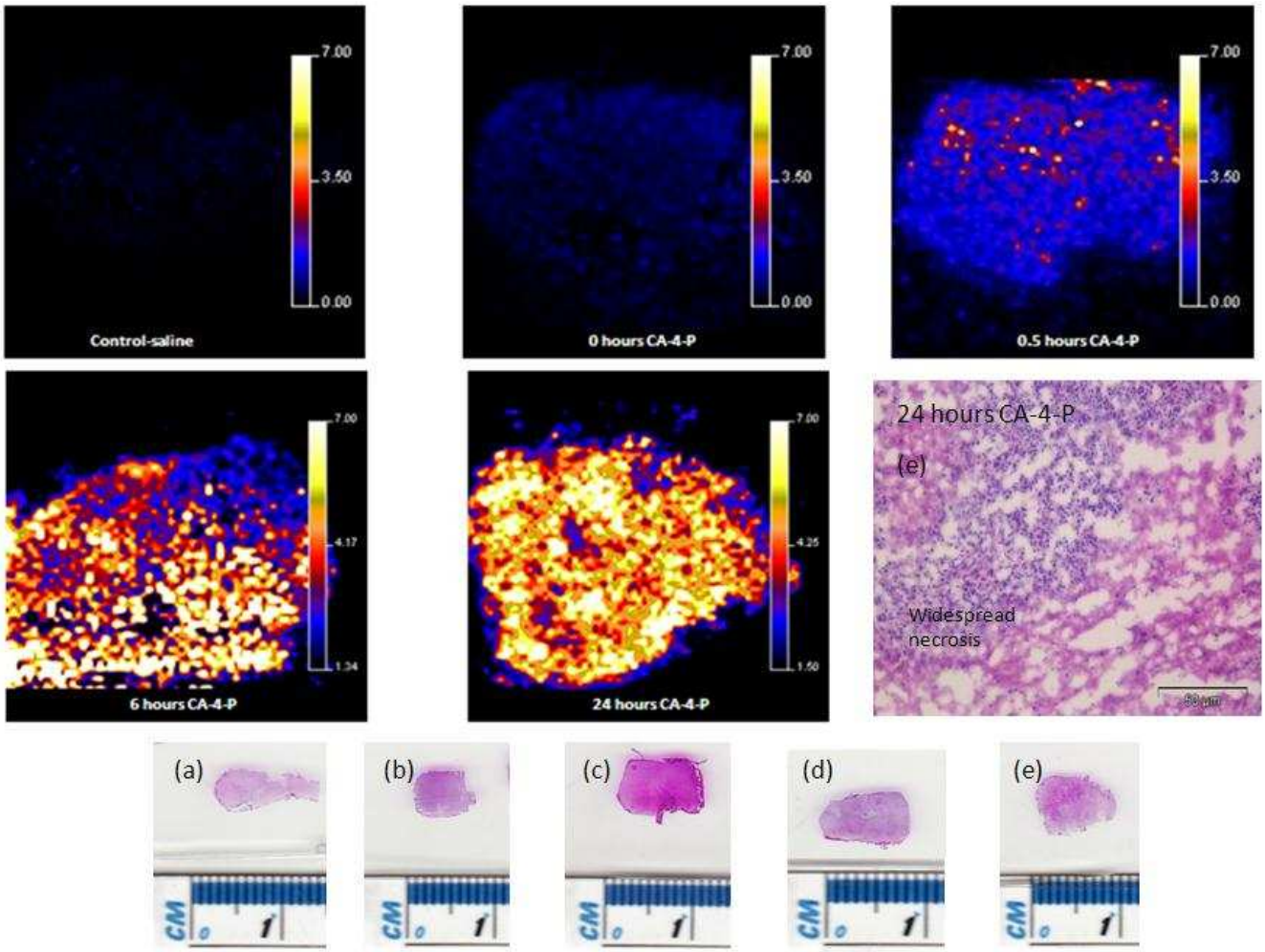

2

3

4

5

6

7

8

9

1 Figure 5

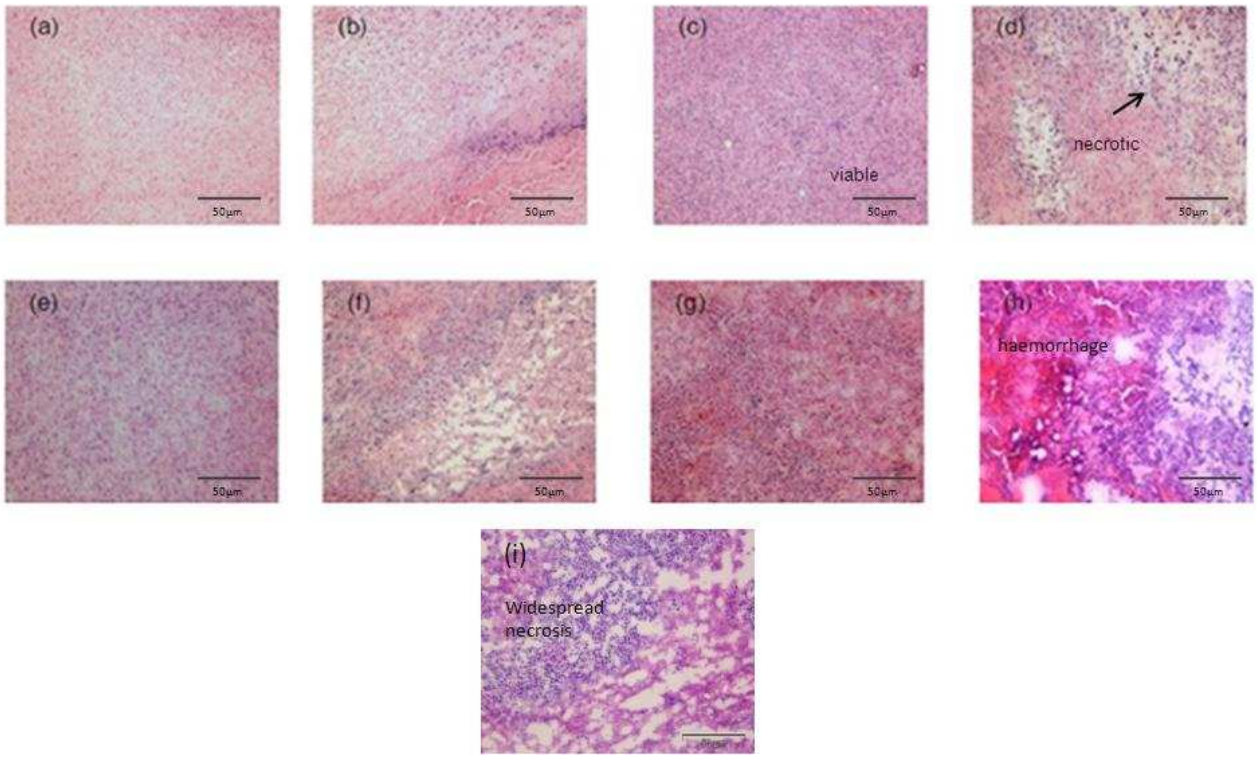

2

3

4

5

6

7

8

9

10

11

1 Figure 6

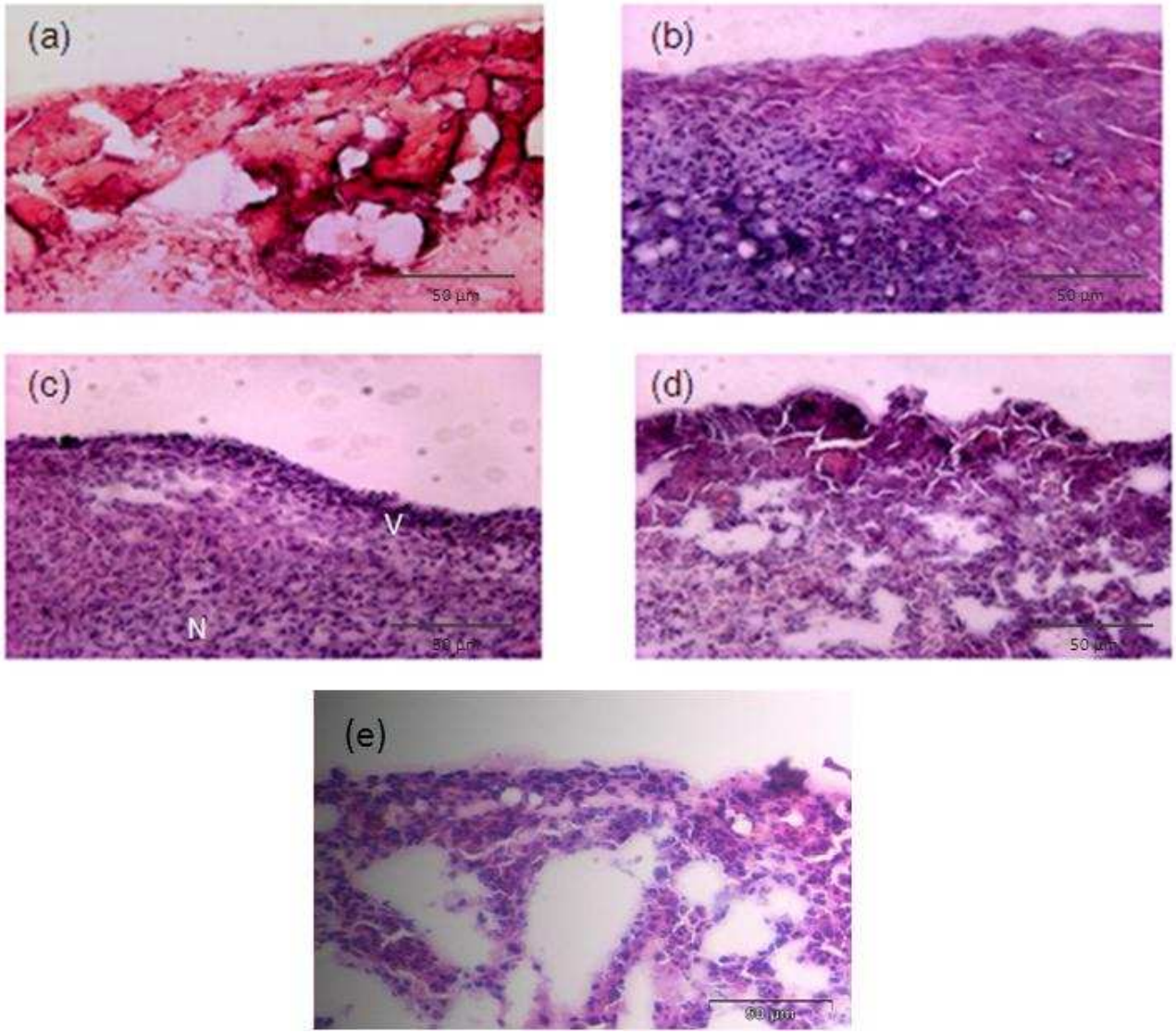

2

3

4

5

6

7

1 Figure 7a

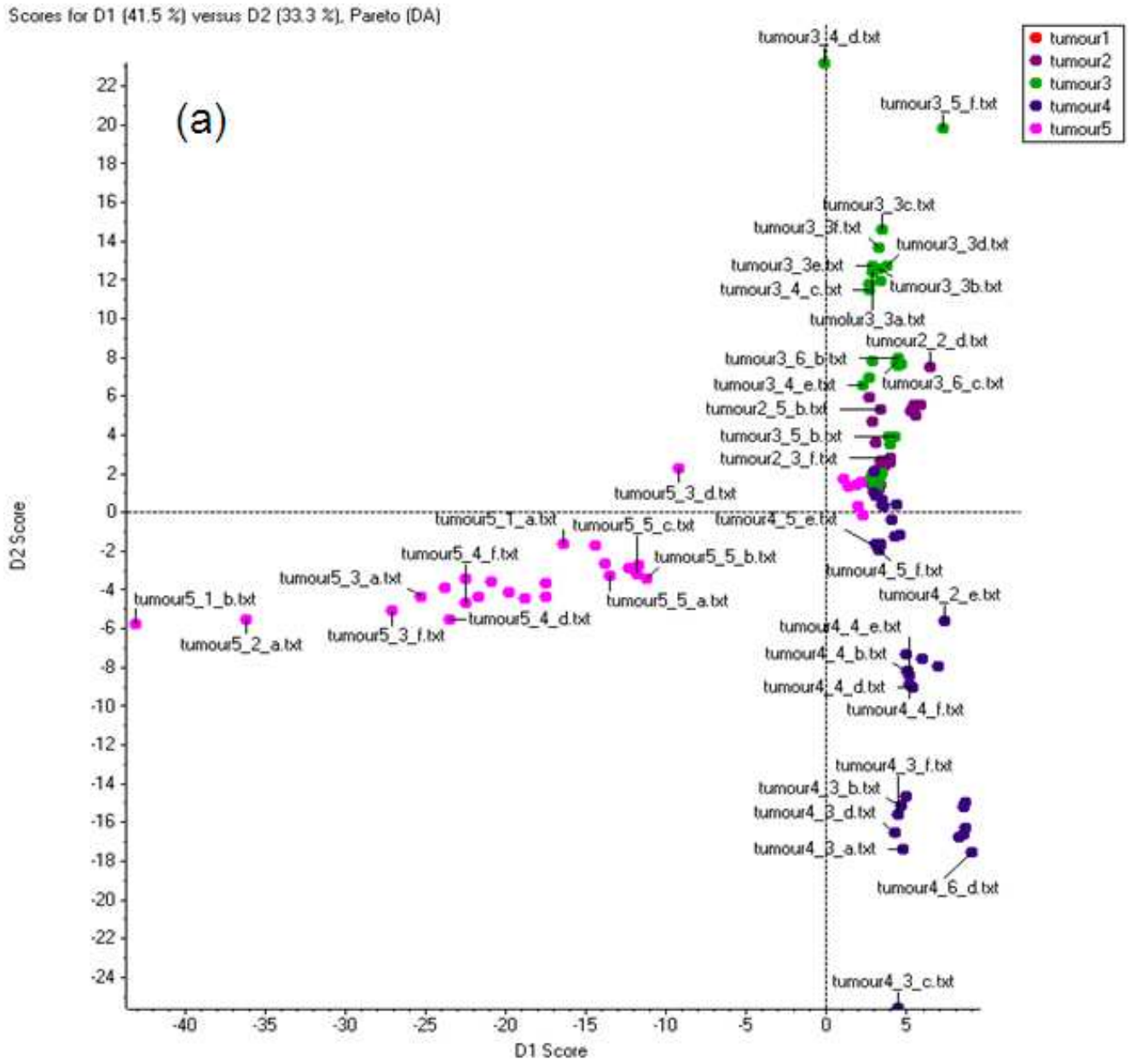

2

3

4

5

6

7

1 Figure 7b

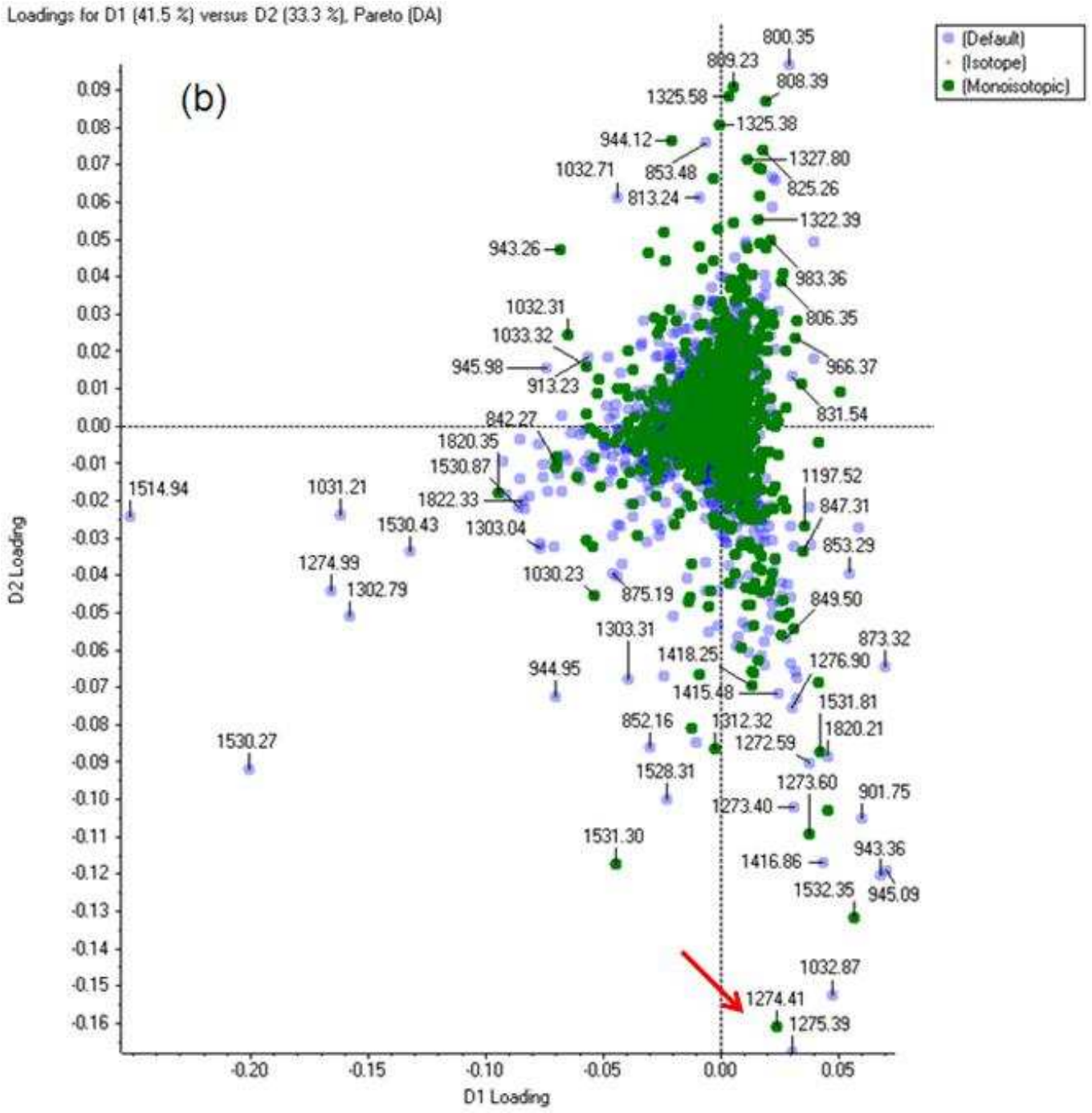

2

3

4

5

Figures 7c

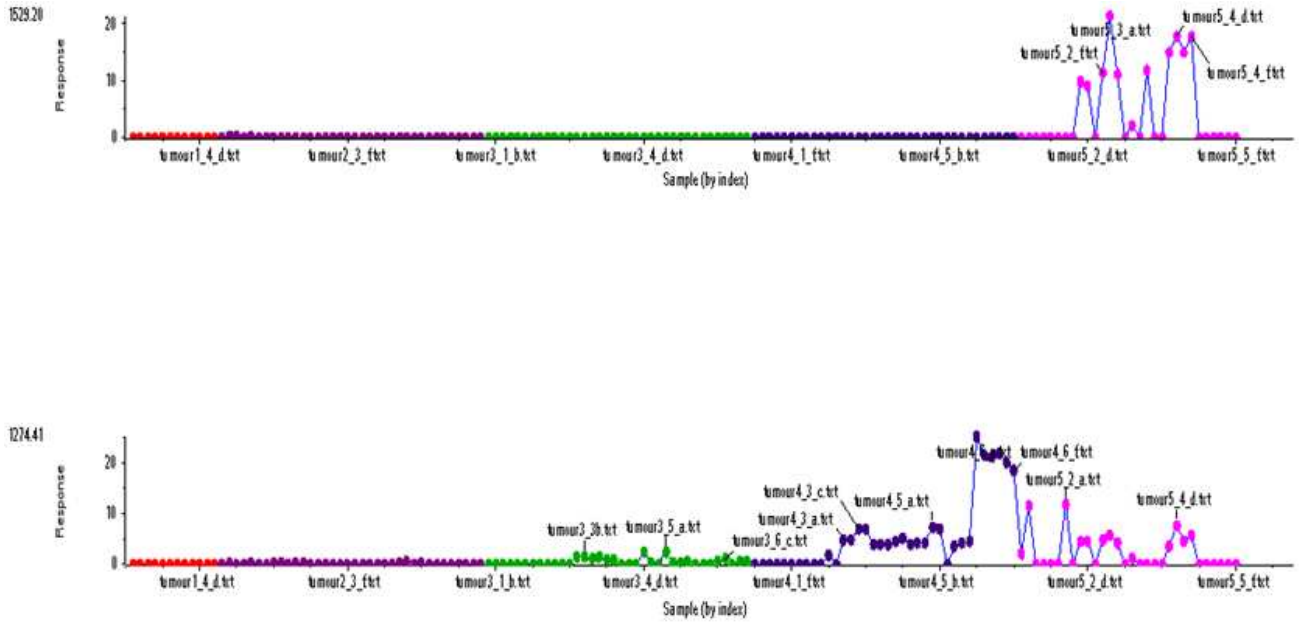
1529.20
Response
20
10
0
tumour1_4_d.txt
tumour2_3_f.txt
tumour3_1_b.txt
tumour3_4_d.txt
tumour4_1_f.txt
tumour4_5_b.txt
tumour5_2_d.txt
tumour5_5_f.txt
tumour5_2_f.txt
tumour5_3_a.txt
tumour5_4_d.txt
tumour5_4_f.txt
Sample (by index)
1274.41
Response
20
10
0
tumour1_4_d.txt
tumour2_3_f.txt
tumour3_1_b.txt
tumour3_4_d.txt
tumour4_1_f.txt
tumour4_5_b.txt
tumour5_2_d.txt
tumour5_5_f.txt
tumour3_2b.txt
tumour3_5_a.txt
tumour3_6_c.txt
tumour4_3_a.txt
tumour4_3_c.txt
tumour4_5_a.txt
tumour4_6_f.txt
tumour5_2_a.txt
tumour5_4_d.txt
Sample (by index)

1 Figure 8

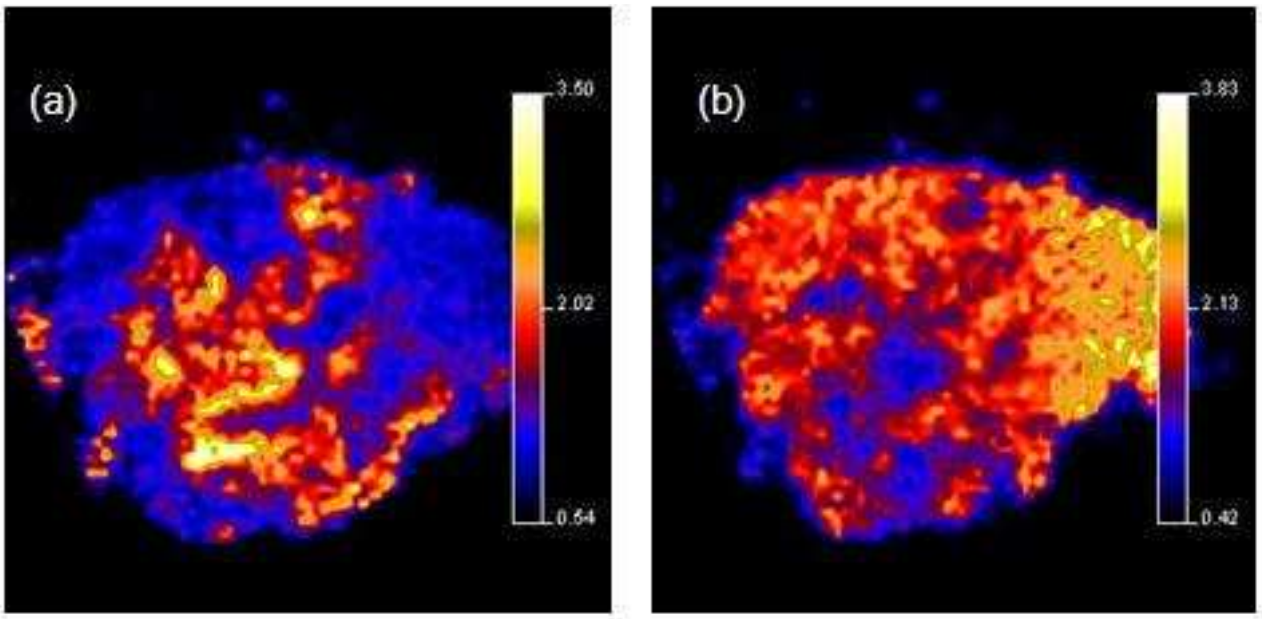

2

3 Figure 9

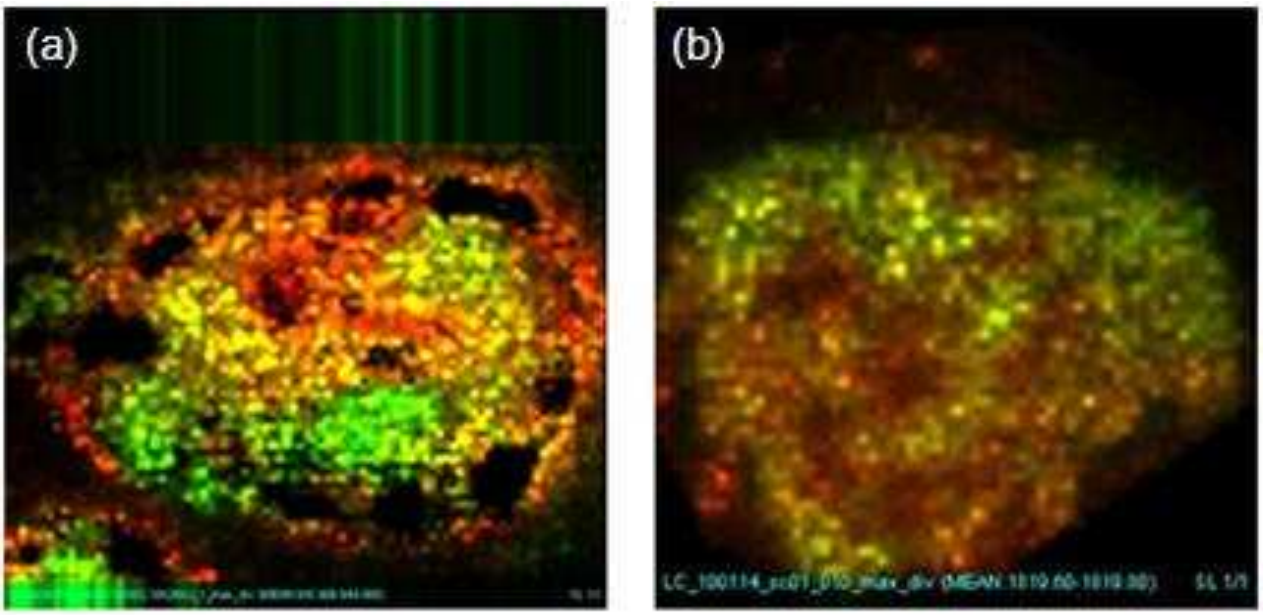

4

5

6